Mon. Not. R. astr. Soc. (1985) **214,** 289–305

Ice in the Taurus molecular cloud: modelling of the 3-μm profile

C. E. P. M. van de Bult and J. Mayo Greenberg *Astrophysics Laboratory, Huygens Laboratorium, Rijksuniversiteit Leiden, PO Box 9504, 2300 RA Leiden, The Netherlands*

D. C. B. Whittet *School of Physics & Astronomy, Lancashire Polytechnic, Preston PR1 2TQ*

Accepted 1984 December 27. Received 1984 December 17; in original form 1984 August 23

Summary. Detailed calculations of the absorption by interstellar core–mantle particles with mantles of different compositions are compared with observations of the 3μm ice band in the Taurus molecular cloud. The strength and shape of the 3-μm band is shown to be a remarkably good diagnostic of the physical state and evolution of the dust in molecular clouds. The strength of the band is consistent with large fractional H_2O mantle concentrations, in the range 60–70 per cent, as predicted by theoretical studies of cloud chemistry and as expected from the high oxygen abundance in pre-molecular clouds.

1 Introduction

The existence of H_2O in grains is now a well-established fact. The most conspicuous evidence has appeared for grains around protostellar sources (Willner *et al.* 1982). The presence of ice in a cold molecular cloud was recently reported by Whittet *et al.* (1983): ice absorption at 3μm was seen in the spectra of stars both within and behind the dark clouds in Taurus, the latter providing the first unequivocal data for molecular cloud material on grains remote from embedded sources. Thus, it is now possible to probe grain composition under more general conditions.

In this paper we shall discuss grain model calculations in detail and try to come to some conclusions concerning the composition, structure, shape and physical state (or history) of the grains as dependent on the shape and strength of the observed 3-μm band. Laboratory spectra of various ice mixtures with various temperature and radiation histories will be used.

2 The grain model

We treat the composition of grains in molecular clouds as having evolved by accretion of 'ice' mantles upon typical diffuse cloud grains with pre-existing organic refractory mantles (Greenberg, van de Bult & Allamandola 1983; van de Bult & Greenberg 1984). To facilitate calculations we represent the compound core – silicate plus organic refractory mantle – as an

average material with a mean index of refraction $\bar{m}\simeq 1.5$. This value is obtained by assuming that the silicate core of 0.05μm radius has an index of refraction $m_{\rm sil}=1.6$ and the organic refractory mantle of radius 0.12μm has an index of refraction $m_{\rm O.R.}=1.45$ (van de Bult & Greenberg 1984). In view of the fact that the organic refractory material has some absorption in the 3-μm region we will approximately represent its effect by considering several possible constant values of the imaginary part of the index of refraction of the compound core.

Both spherical and elongated particles (represented here by infinite circular cylinders) will be taken as extreme cases of variation in shape. It is to be expected that the cylindrical model should be more consistent with observation since, in general, interstellar grains show polarization, and the presence of polarization structure in the 3-μm ice band indicates that the ice mantles are on these non-spherical particles (Dyke & Lonsdale 1981).

3 Data handling

A flux curve showing a broad absorption band is shown in Fig. 1 as $\log F$ versus wavelength λ. This is converted to an extinction by subtracting it from $\log F_0$, the source spectrum.

The attenuation can be separated into a constant dilution factor due to distance and an optical depth τ_λ which consists of: (i) a background continuum extinction which may or may not be due to particles responsible for the absorption band, and (ii) extinction due to the core–mantle–mantle grains, which give the absorption feature.

The shape and strength of narrow absorption features are readily obtained by simply connecting the continuum at both ends to obtain the baseline. However, for broad features this procedure may introduce errors, which are compounded in the case of the 3-μm band by the presence of strong telluric absorption at the short wavelength end of the profile. These errors, when significant, can be easily quantified.

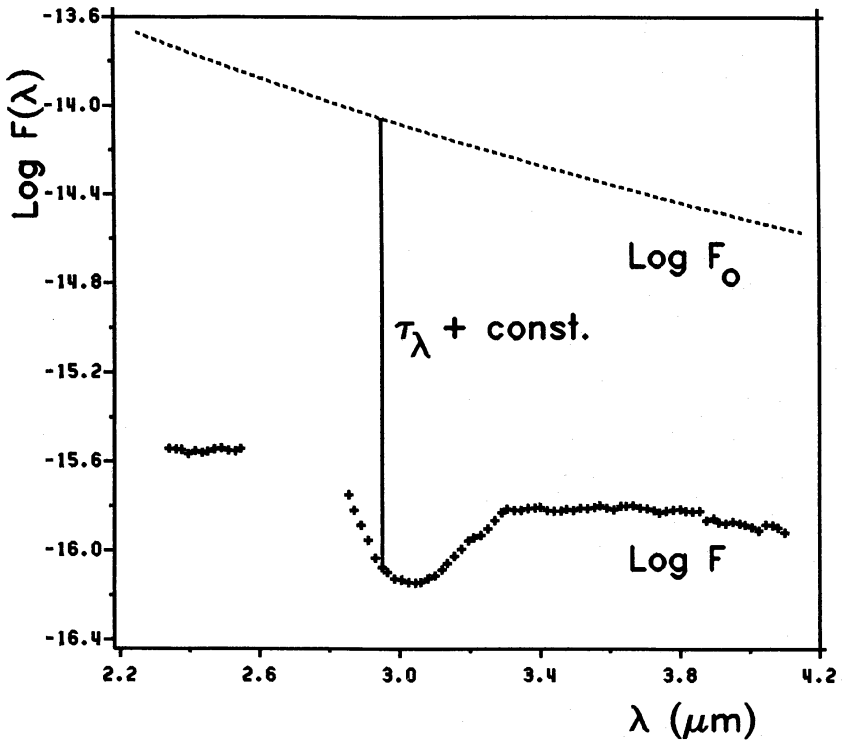

Figure 1. Illustration of the total attenuation in the 3-μm region presented as the difference between a source spectrum, $\log F_0$, (4580K blackbody), and an observed spectrum (Elias 16).

Our procedure for handling the data is based on the following steps:

(i) In the wavelength range of interest the background source is approximated by a straight line. We represent the radiation from the source by a blackbody. If the temperature of the blackbody is high enough (say above 1500K) that the maximum of the curve is well below the wavelength range of interest, the effect of linearization between 2.5 and 3.8μm is to introduce an underestimate in the strength (optical depth) of the ice band of no more than 0.04. At a temperature of about 2000K the effect is zero and at higher temperatures there is a small overestimate. For lower temperatures, however, the effect increases so that for, say, 1000K, $\Delta\tau\sim0.11$. These effects are independent of the total amount of extinction and are therefore quite important for weak ice bands and low-temperature background sources.

(ii) The background extinction outside the absorption band, whether due to the particles responsible for the ice band or due to various combinations with other particles such as carbon, will be represented by a straight line. In actuality there is some curvature of the extinction law variously estimated to be given by $\lambda^{-\alpha}$, where α is of the order of 2. We consider the specific case given by $\alpha=1.85$ (Landini *et al.* 1984) to obtain an estimate of our correction. In this procedure we underestimate the optical depth. This effect is proportional to the total extinction. Using an extinction law $\tau_\lambda/A_V=0.337\times\lambda^{-1.85}$, as deduced from the data presented in Landini *et al.* (1984), we calculate a maximum deviation $(\Delta\tau)_{max}/A_V=0.006$.

The sum of the effects of the two linearizations is that the overall continuum flux values are connected by a straight line running from $\lambda\simeq2.5$ to $\simeq3.8\mu$m and the difference between this background and the observed flux is taken as defining the extra absorption within the 3-μm feature.

4 Model calculations

Calculations have been made for core–mantle spheres and infinite circular cylinders using exact theoretical methods (see e.g. Kerker 1969; Shah 1970). For spheres in the size range appropriate to normal interstellar grains, the scattering is negligible so that the extinction is given almost completely by the absorption. For cylinders of the same diameter, on the other hand, a scattering term appears which has been shown to be an artifact of the infinite length when compared with the

	Compound core			Mantle	
	radius a_{cc} (μm)	index of refraction m'_{cc}	m''_{cc}	radius a_m (μm)	mixture [a]
Spheres:	.12	1.5	0,0.05,0.1	.132	1u,1a,2u,2a
	.12	1.5	0,0.05,0.1	.14	1u,1a,2u,2a
	.20	1.5	0,0.05,0.1	.22	1u,1a,2u,2a
	.20	1.6	0.001	.22	1u,1a,2u,2a
Cylinders:	.12	1.5	0,0.05,0.1	.132	1u,1a,2u,2a
	.12	1.5	0,0.05,0.1	.14	1u,1a,2u,2a

[a] mixtures 1 and 2 specify pure H_2O and H_2O:NH_3 = 3:1; u and a designate unannealed and annealed mixtures respectively.

results of very long spheroids. This has been discussed Greenberg *et al.* (1983). For this reason we ignore the scattering contribution to the extinction, and the absorption alone is assumed to be a good approximation to the extinction by elongated particles in this size range.

Table 1 shows most of the models we have tested. We note here that the amount of NH_3 in the 3:1 mixtures is unquestionably too large to be a proper representation of the interstellar medium. But these are examples of mixtures for which exact optical properties have been deduced by appropriate Kramers–Kronig analysis for both unannealed and annealed samples (Hagen, Tielens & Greenberg 1981, 1983a). In lieu of having an appropriately diluted mixture we have assumed (as a first approximation) that a possible compound which produces the wing is NH_3 (H_2CO may be another candidate) and that the maximum strength of the 3.07μm depth may be scaled by the fraction of H_2O in the mixture (Greenberg 1982a, b).

We apply step two of Section 3 to arrive at a standard baseline for all calculated extinction curves which encompass the absorption band. Thus we draw a straight line between the calculated $Q(\lambda_{min})$ and $Q(\lambda_{max})$ where λ_{min} and λ_{max} are clearly outside the wavelength range of the absorption band. After the baseline subtraction has been done, both the observed and the calculated absorption bands are reduced to profiles which now have a zero baseline.

The profiles derived from the model calculations are multiplied by a scaling factor S to match with the depth of the observed band. This scaling factor is $S=N\pi a^2$ for spheres or $S=N4ea^2$ for cylinders of elongation e where N is the column density of grains. The optical depth is then $S\times Q_{ext}(\lambda)$.

5 Effects of grain parameters on band shapes

In this section we shall discuss the effects of changing the parameters in our model calculations. We consider: (5.1) changing the mantle H_2O concentration and changing the shape of the particle, i.e. spherical versus cylindrical, (5.2) adding an imaginary component to the index of refraction of the core (core absorption), and (5.3) increasing the size of the particles (core plus mantle) or the mantle alone. It will be seen that the effects of (5.2) and (5.3) are of minor importance. Where useful we use a specific observation for comparison.

5.1 EFFECT OF MANTLE COMPOSITION AND SHAPE

We combine the consideration of mantle material and shape because they are inextricably connected (see Greenberg *et al.* 1983).

In Fig. 2a, b are shown the results of our calculations for the spherical, compound core–mantle particles with $a_{cc}=0.12\mu$m and $a_m=0.132\mu$m, and $m_{cc}=1.5-i0.0$ for the following mantle mixtures: 1u – pure H_2O amorphous ice, deposited at 10 K; 1a – the same but after annealing to 80 K; 2u – a mixture H_2O:NH_3=3:1, deposited at 10 K; and 2a – the same but after annealing to 50 K. These results are compared with the observations for HL Tau by Whittet *et al.* (1983).

In Fig. 3a, b the results for the cylindrical particles are presented, all other parameters being the same as in Fig. 2a, b.

Pure unannealed ice (mixture 1u). For spheres and cylinders we find a rather symmetric band with full widths at half maximum (FWHM) of 0.30μm, equivalent to 330 cm^{-1}. The short and long wavelengths of the onset of the band are the same but for cylinders the band is tilted with respect to that for spheres; its maximum is therefore shifted toward longer wavelengths: 3.01μm for spheres and 3.07μm for cylinders.

Pure annealed ice (mixture 1a). For this mixture the band, as calculated for spheres, is narrower than the band of the unannealed mixture (FWHM is 0.275μm, equivalent to 300 cm^{-1}), especially

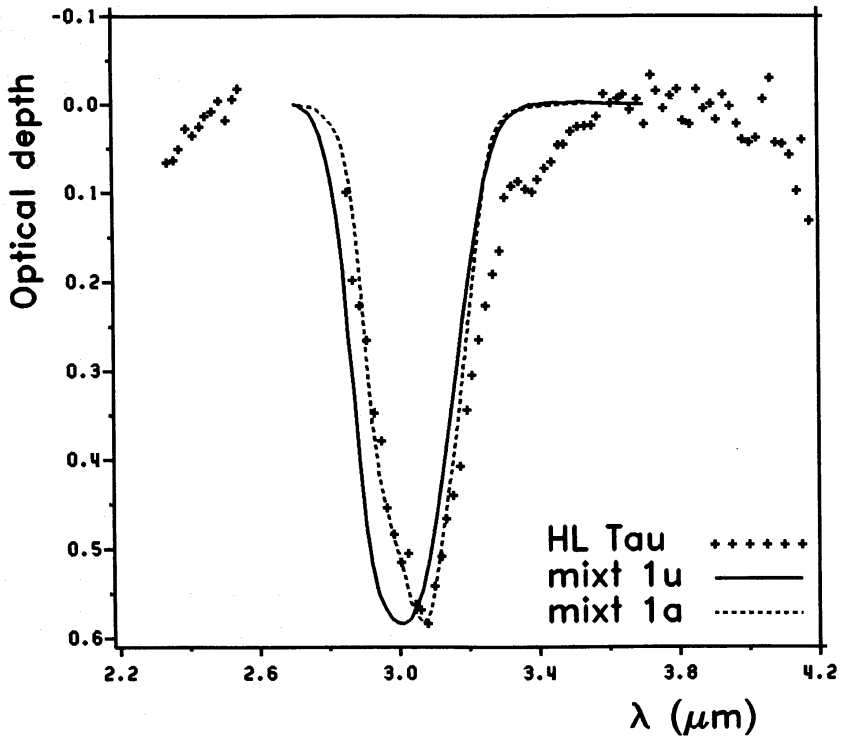

(a)

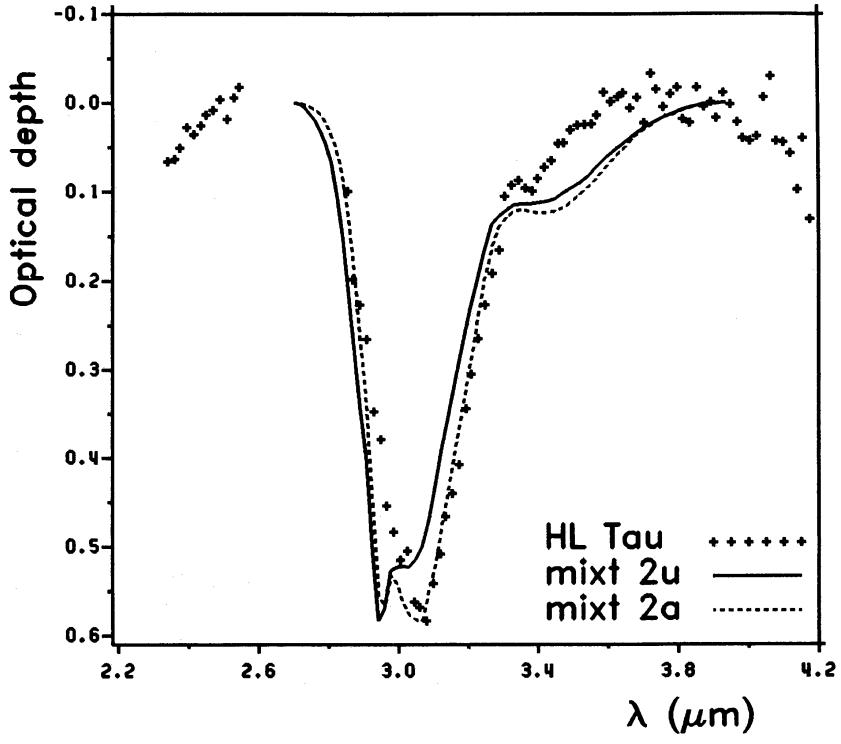

(b)

Figure 2. Absorption by spherical compound core–mantle particles with $a_{cc}=0.12\mu$m and $a_m=0.132\mu$m. Mantle mixtures, mixt 1 (Fig. 2a) and mixt 2, (Fig. 2b) are respectively pure H_2O and H_2O:NH_3=3:1. Unannealed and annealed are denoted by u and a. Core absorption $m''_{cc}==0$. Comparison is with HL Tau.

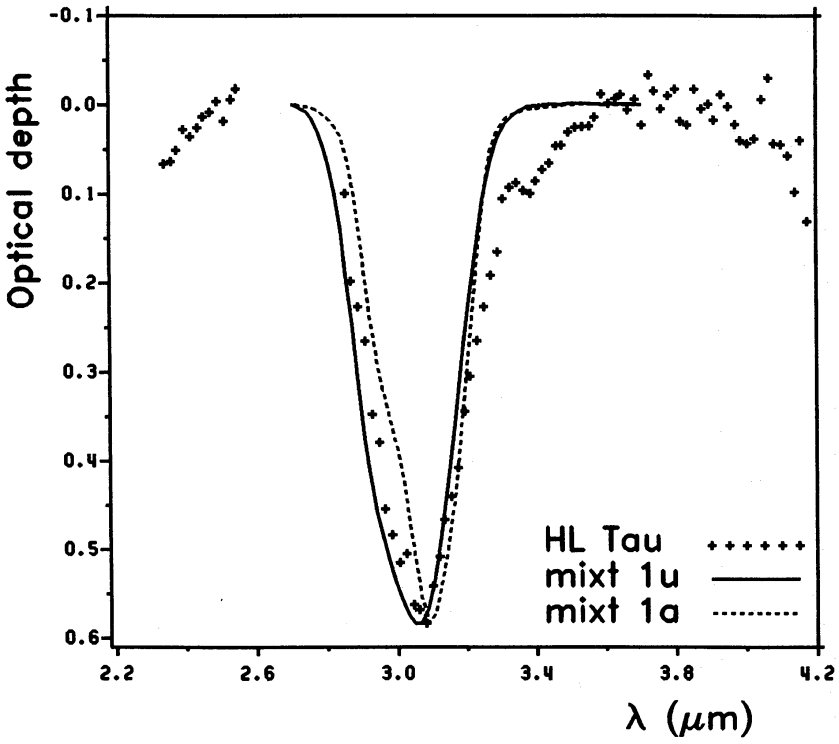

(a)

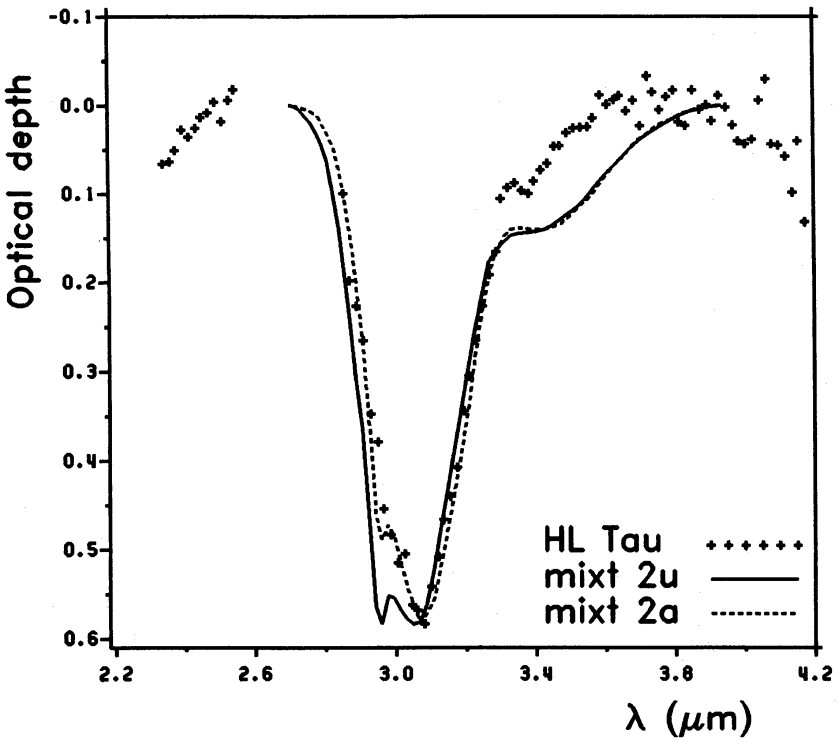

(b)

Figure 3. Same as Fig. 2 but for cylinders.

at the peak of the absorption. The peak is shifted towards longer wavelength, 3.07μm. The band shows two inflections at the short wavelength side.

At short wavelengths up to about 3.1μm, this band fits the observed profile of HL Tau rather well; however it lacks the absorption wing at longer wavelengths. In general it is impossible to get a wing using pure H_2O ices for particle sizes typical of interstellar grains.

The cylinder band is much narrower (FWHM 0.25μm or 270 cm^{-1}) and tilted with respect to the sphere; its maximum is at 3.09μm.

The unannealed mixture H_2O:NH_3=3:1 (mixture 2u). For spheres the band has a sharp peak at 2.94μm due to the N–H stretch in NH_3 and a broader one at 3.03μm due to the H_2O. The NH_3 absorption is much deeper than that of H_2O. The wing at long wavelengths is too strong to explain the observations.

The band profile calculated for cylinders shows again two absorption peaks, but now of equal depth – the NH_3 is suppressed with respect to the H_2O. The peak absorptions are at somewhat larger wavelength, 2.96 and 3.05μm respectively. The long-wavelength wing is about 20 per cent stronger than that calculated for spheres.

The annealed mixture H_2O:NH_3=3:1 (mixture 2a). Both for spheres as well as for cylinders the absorption due to NH_3 is suppressed with respect to that due to H_2O, when compared with the unannealed mixtures. For spheres the strength of the peak absorption due to NH_3 (at 2.96μm) is somewhat less than that due to H_2O (at 3.07μm); for cylinders the extra peak at 2.96μm is *just* detectable at the short-wavelength side of the band; in this case the H_2O absorption peaks at 3.07μm. The long-wavelength wing of the sphere band is about 10 per cent stronger than that calculated for the unannealed mixture; for cylinders the wings are equally strong for both mixtures.

Apart from the wing being too strong, and the small extra dip at 2.95μm, the shape of the cylinder band represents the HL Tau observations rather well, suggesting that a mixture with less NH_3 could match the observations.

In general for equivalent mixtures elongated particles give an increased absorption at the longer wavelength side of the band relative to the short wavelength side as compared with the result for spheres.

5.2 EFFECT OF ABSORPTION IN THE CORE

In Fig. 4 are shown the results for the spherical, compound core–mantle particles with a_{cc}=0.12μm and a_m=0.132μm and with the annealed H_2O:NH_3 mixture as a mantle for demonstrating the effect most clearly. The complex index of refraction of the core is, for the two curves, given by $m_{cc}=1.5-i0.0$ and $m_{cc}=1.5-i0.1$ respectively. These results are again compared with the observations by HL Tau.

It is to be remarked that adding an absorption to the core results in a slight decrease of the wing at the long-wavelength side of the absorption band. In general the extinction at longer wavelengths decreases, but for the pure ice mantles (1u and 1a) this produces only a marginally observable effect. Increasing the mantle thickness (a_{cc}=0.12 and a_m=0.14μm) further reduces the relative effect of core absorption. Increasing the particle sizes, core and mantle together but keeping the ratio a_{cc}/a_m constant (a_{cc}=0.20 and a_m=0.22μm) does not influence this effect.

Using cylindrical particles reduces the effect of adding absorption to the core relative to the spherical particles. Increasing the overall size of the particles, but keeping a_{cc}/a_m constant, or increasing the mantle alone appears to lessen the effect of core absorption which was already negligible.

We have also calculated the extinction for an increased real index of refraction of the core: m_{cc}=1.6 (with m''=0.001) with no observable change in the shape of the band.

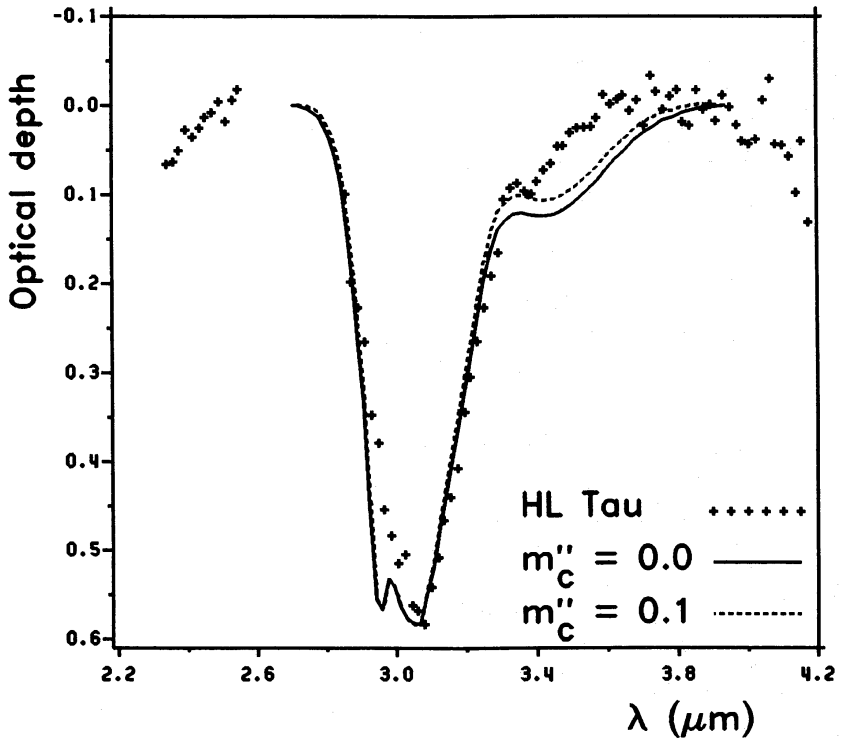

Figure 4. Comparison of absorption by spherical compound core–mantle particles with $a_{cc}=0.12\mu$m and $a_m=0.132$ for annealed $H_2O:NH_3=3:1$ mantle mixture and core absorptions $m''_{cc}=0.0$ and 0.1.

In summary then, varying the core absorption or the real part of the index of refraction by moderate amounts produces at most very small changes in the *shape* of the calculated absorption band. Of course modifying the core absorption will provide, in effect, a different baseline for the extinction and consequently produce variations in the *depth* of the absorption feature. In terms of our method of reduction this implies a different scaling factor. But the maximum change in the scaling factor resulting from adding core absorption is quite small, being less than ~3 per cent.

5.3 EFFECT OF SIZE

When there is no absorption in the core, scaling the size of the particle (core plus mantle) or mantle alone does not produce any change. When there is core absorption there is an effect, already discussed in Section 5.2, of a marginal decrease in the log-wavelength wing.

In summary, with the normalization procedure adopted here the only parameters which significantly modify the shape and strength of the absorption band are the basic ones of mantle composition and shape of the particle. If we assume that all particles are elongated, then the mantle material alone provides the discriminant in comparing observations with theory. For this reason, in the following we consider only core–mantle cylinders with $a_{cc}=0.12\mu$m and $a_m=0.132\mu$m and $m_{cc}=1.5-i0.0$ for comparison with the observations.

6 Comparison with observations

Of the stars observed by Whittet *et al.* (1983), those most suitable for detailed comparisons with the models are HL Tau and Elias 16, as they have greater optical depth in the 3-μm feature as well as good signal-to-noise. The scatter in the 3-μm profiles obtained for other sources, largely due to the weakness of the absorption feature, precludes any definite conclusions, but it is possible to arrive at some suggestive estimates of the grain mantles.

Limiting ourselves to cylinders we study the different absorption profiles of various stars in detail.

HL Tau. A suggestive fit is given by the annealed H_2O:NH_3=3:1 mixture (see Fig. 5). However we note that this composition gives too strong a wing as well as too distinctive a 2.96-μm feature. We can clearly conclude that the actual amount of NH_3 in the grains must be much less than 25 per cent.

As already noted in Greenberg *et al.* (1983) the shape of the absorption band produced by cylinders closely matches the material absorption m''. This permits us to look directly at the absorption by various mixtures in bulk to get an estimate of the variation of shape with NH_3 concentration without doing further grain model calculations. In Fig. 6 we show both the 10 and 25 per cent NH_3 in H_2O mixtures in the same scale to compare with the observation.

The absorption strength deduced from Fig. 5 is 0.58. Note that the combined effect of the linearization of the blackbody source and of the background extinction in this case is to lower the value we get by 0.08 Therefore our best estimate for τ_3 is 0.66, assuming a blackbody temperature of 1100K and A_V=8.

Elias 16. The 3-μm band of Elias 16 is measurably wider than that of HLTau, indicating an unannealed mixture (see Fig. 7). Again both the observed wing and 2.95-μm feature are much weaker than in the 25 per cent NH_3 mixture (see Fig. 8). This again can be explained by a reduction in the NH_3 concentration (see Fig. 9). The directly deduced strength is 1.09; the corrected strength based in a blackbody temperature of 4580K and A_V=20.6 is 1.19.

XZ Tau. This star has no measurable ice band.

Elias 1. In Fig. 10 we present the comparison of the calculated 3-μm absorption spectrum and Elias 1. From the width of the line we conclude that this is an unannealed ice. The emission features at 3.4 and 3.5μm make it difficult to assess the presence of a wing; however, the cluster of

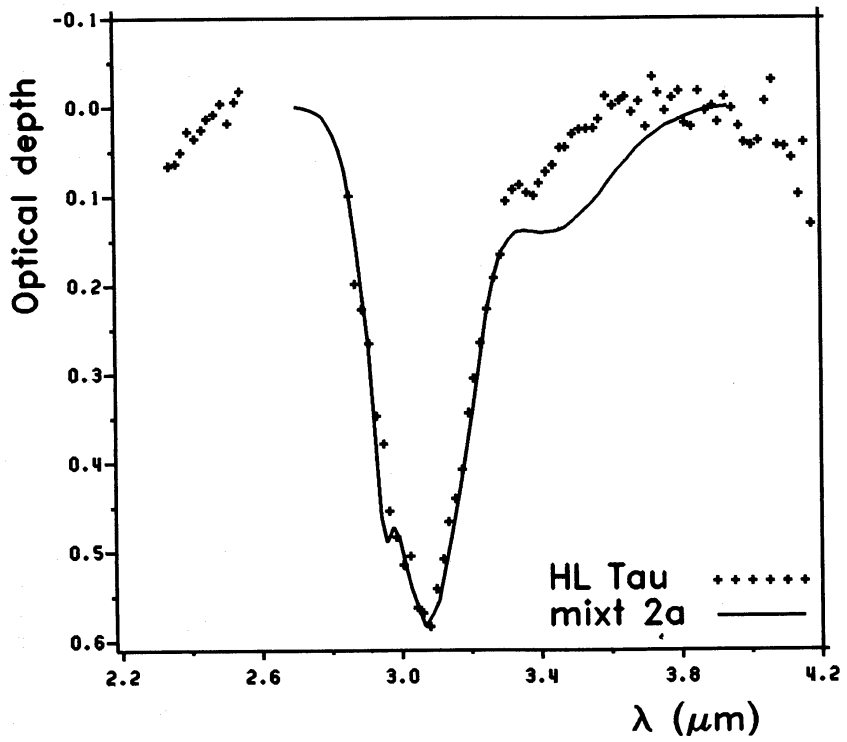

Figure 5. Comparison of absorption by cylinders having annealed mantles of H_2O:NH_3=3:1 with observations of HLTau. a_{cc}=0.12μm, a_m=0.132μm.

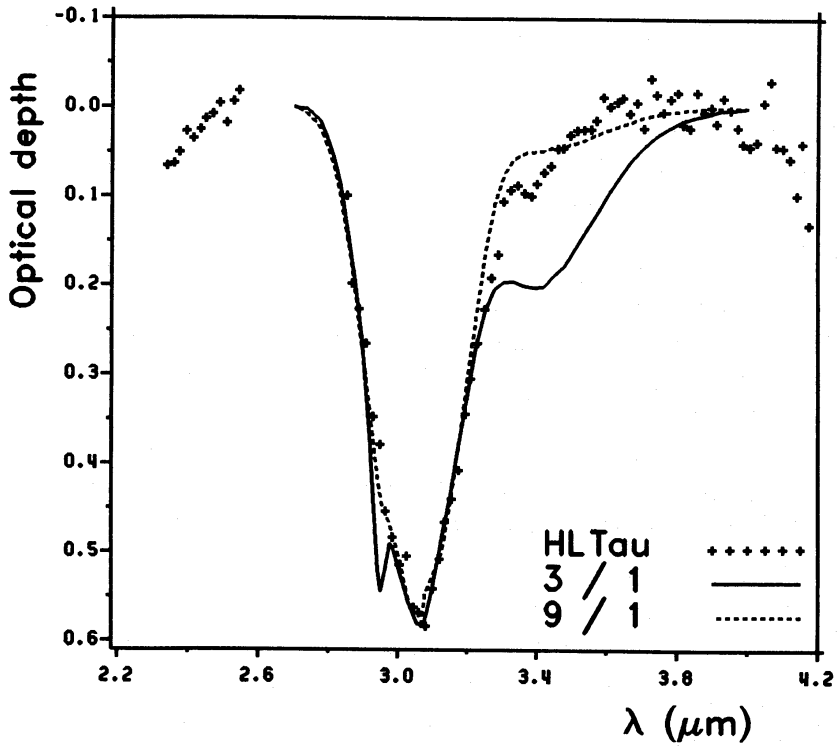

Figure 6. Comparison of laboratory measurements of absorption for bulk annealed H_2O:NH_3=3:1 and H_2O:NH_3=9:1 with observations of HL Tau showing the decrease of the 2.96-μm structure and the long-wavelength wing with decreasing NH_3 concentration.

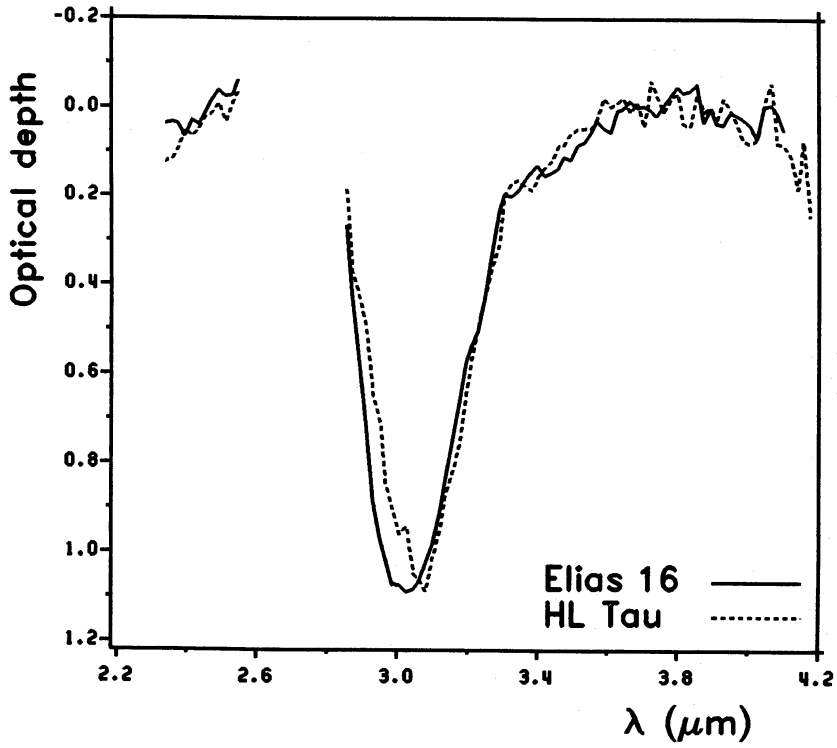

Figure 7. Comparison of the observed spectra of HL Tau and Elias 16 normalized to the same optical depth and with straight lines connecting the points.

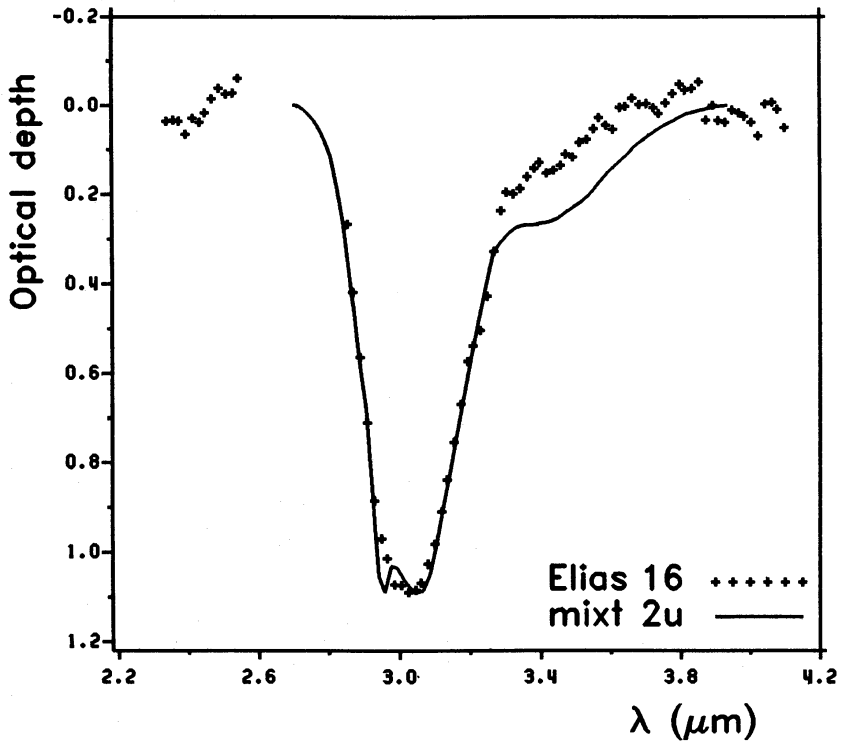

Figure 8. Comparison of absorption by cylinders having unannealed mantles of H_2O:NH_3=3:1 with observations of Elias 16. a_{cc}=0.12μm, a_m=0.132μm.

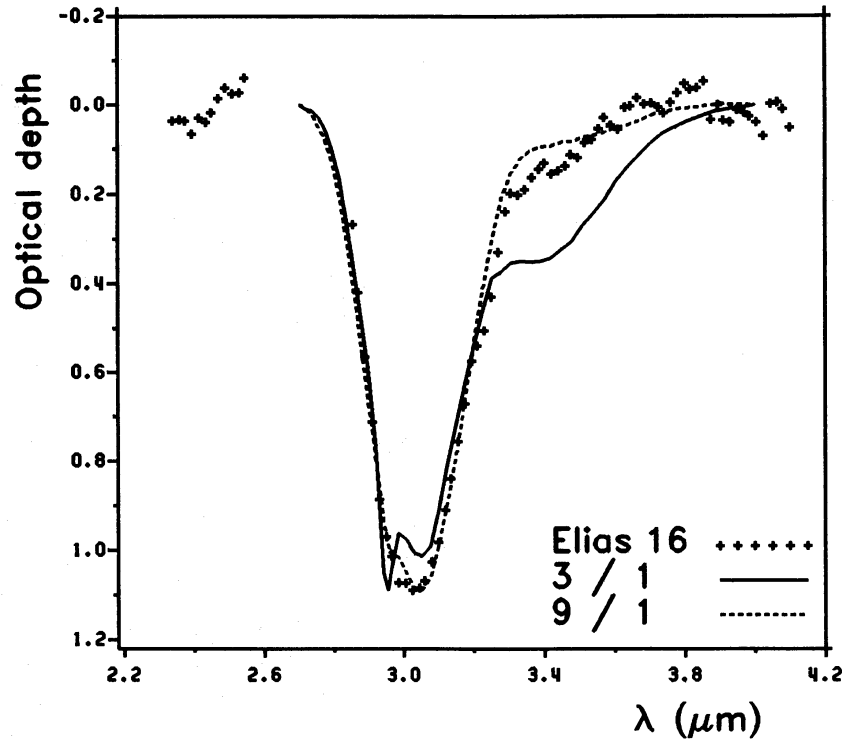

Figure 9. Comparison of laboratory measurements of absorption for bulk unannealed H_2O:NH_3=3:1 and H_2O:NH_3=9:1 with observations of Elias 16 showing the decrease of the 2.96-μm structure and of the long-wavelength wing with decreasing NH_3 concentration.

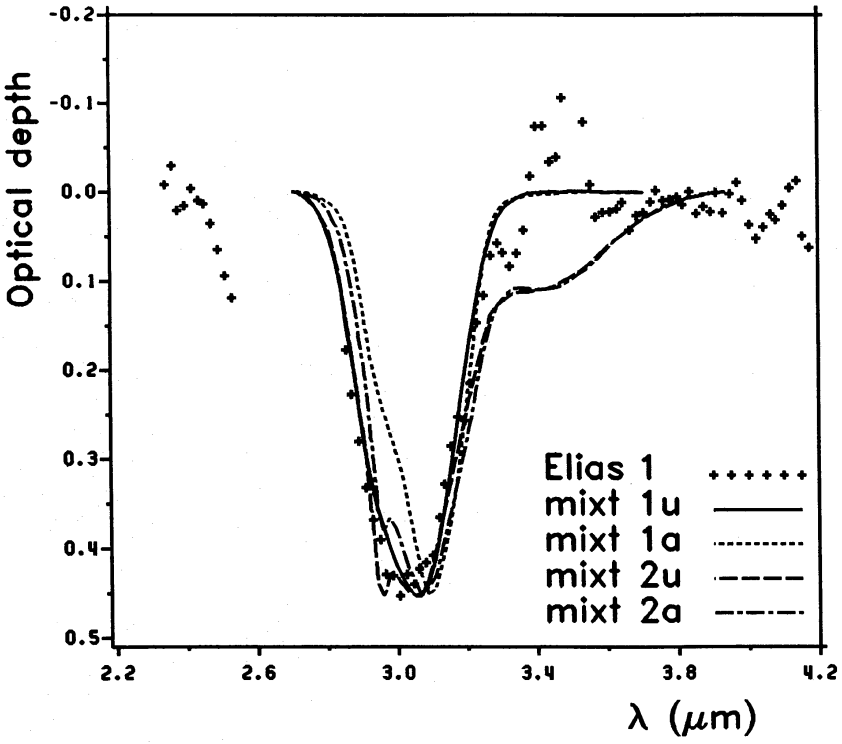

Figure 10. Comparison of Elias 1 observations with absorption by cylindrical compound core–mantle particles with $a_{cc}=0.12\mu$m and $a_m=0.132\mu$m. Mantle mixtures, mixt 1 and mixt 2, are respectively pure H_2O and $H_2O:NH_3=3:1$. Unannealed and annealed are denoted by u and a. Core absorption $m_c''=0$.

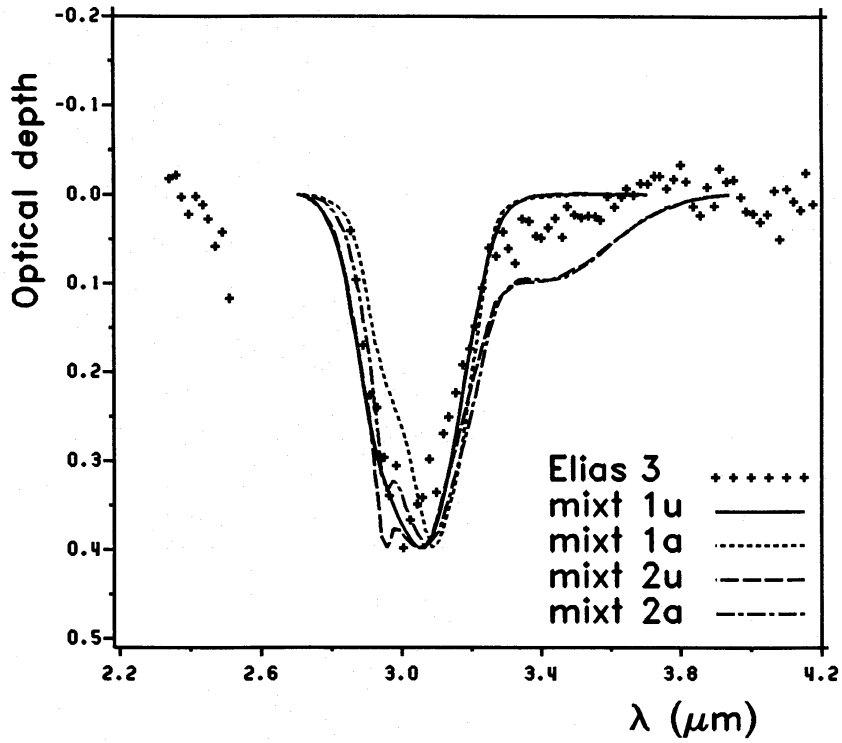

Figure 11. Same as Fig. 10 for Elias 3.

points in the 3.3-μm region and the return to the background at about 3.6μm gives some indication that there may be an absorption wing underlying the emission. At 2.96μm there is no definite structure outside the noise. We conclude therefore that Elias 1 is similar to Elias 16. However given the uncertainties concerning the wing the shape is also consistent with an almost pure H_2O ice.

The strength of the band is 0.45; the blackbody correction assuming a temperature of 1500K is about 0.011; the extinction correction is 0.054 so the corrected strength is 0.52.

Elias 3. This spectrum (see Fig. 11) is noisy in the region of maximum absorption. The presence of the wing is a reasonable supposition here, but the profile has too much scatter, particularly at its peak, to allow any confident statements to be made concerning the width of the band. It seems safe to say that it is clearly not pure annealed H_2O ice, such as that of Leger *et al.* (1983).

The strength is somewhere between 0.35 and 0.40. The blackbody correction is -0.025 and the extinction correction is about 0.05, so the corrected strength is in the range $0.37-0.43$.

Elias 6. It is notable for this star that the position of maximum absorption in all of our model calculations, except perhaps the unannealed mixture, occurs at significantly larger wavelengths than that of the observed maximum (see Fig. 11). The width of the feature indicates an unannealed ice and the wing is very indistinct.

The strength of the band is 0.39; the blackbody correction is -0.02, the extinction correction is 0.04, so the corrected strength is 0.41. In this late-type star the blackbody correction is not completely adequate and, in fact, using the actual stellar emission gives a slightly smaller value of τ_3 because it has a slight intrinsic dip at around 3μm (Merrill & Stein 1976).

Elias 9. The 3-μm feature is very weak in this source, hence the profile is extremely noisy. If we exclude the lowest observed point the shape of the band is closest to that of an unannealed ice mixture (Fig. 13).

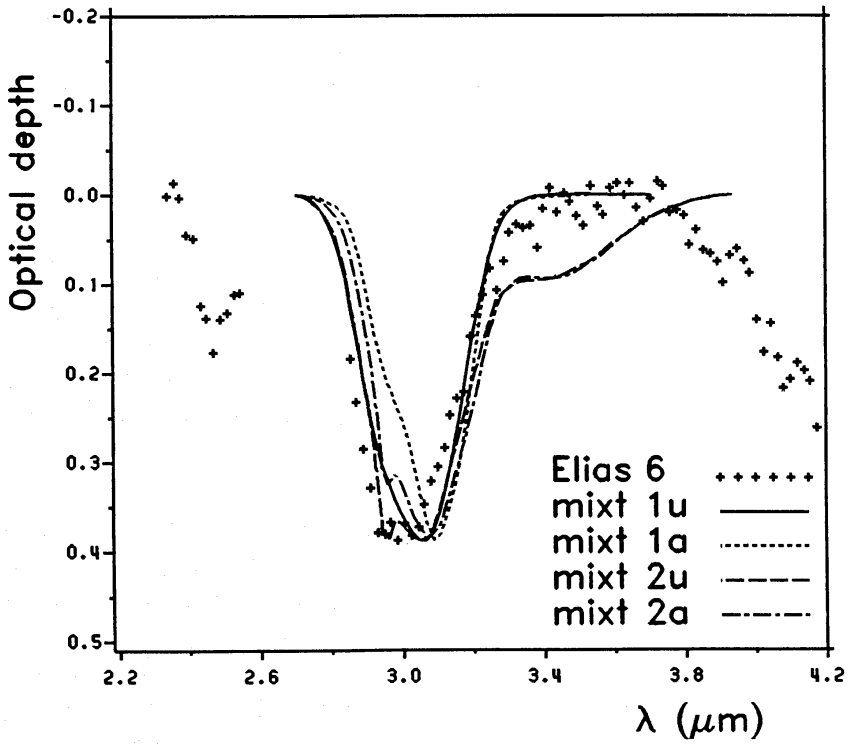

Figure 12. Same as Fig. 10 for Elias 6.

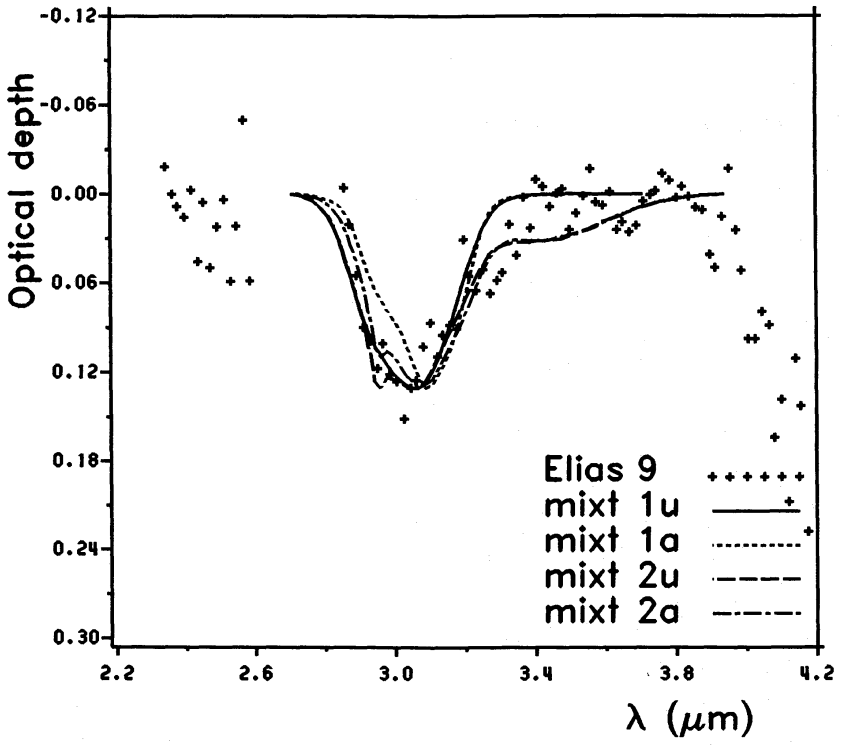

Figure 13. Same as Fig. 10 for Elias 9.

The strength of the band is 0.13; the blackbody correction is −0.02, the extinction correction is 0.03 so the net depth is 0.14. As for Elias 6, the actual depth should be slightly reduced because of the small error introduced in representing the stellar emission by a blackbody.

An overall view of the comparison between calculations and observations shows that:

(i) pure ice cannot provide the basically ever present long-wavelength wing;
(ii) the wing in the H_2O:NH_3=3:1 mixture is always too large;
(iii) the structure implied by the H_2O:NH_3=3:1 mixture at =2.95μm is much larger than the observed fine structure, if it exists at all.

7 Discussion

HL Tau is a dust embedded star; according to Cohen (1975, 1983) it is extremely young with an edge-on disc and a significant amount of local dust. It seems certain that this dust has been modified by physical processes which are not relevant to most of the dust in a normal molecular cloud. Consequently it is not surprising to find that the narrowness of the band shape indicates that some annealing has taken place which would be consistent with the local higher temperature of the grains (Cohen 1983).

Both the width and peak position of the observed band are remarkably well reproduced by the absorption spectrum calculated for cylindrical particles with either mixture (H_2O:NH_3=3:1 or 9:1). By comparing the calculated absorption spectrum in Fig. 5 for the 3:1 mixture and the direct bulk absorption for the same mixture in Fig. 6 we deduce that the effect of the particles is to reduce the long-wavelength wing by about 0.13/0.2 (note an even greater effect on the 2.96-μm structure). From this we estimate that the wing 'plateau' for a 9:1 mixture would be reduced from that shown in Fig. 6 to a 'calculated' value in Fig. 5 of about 0.03. Since the observed mean plateau is about 0.09 we arrive at a 'best guess' intermediate mixture ratio (interpolating between 0.03 and 0.13) to be about 6:1. This is the kind of ratio we expect to find in grain mantles derived from

theoretical calculations of the chemical evolution of dust and gas in clouds. Consideration of time-dependent interactions including not only ion–molecule reactions but also grain surface accretion, migration, radiation and ejection by grain explosions leads generally to H_2O-rich grain mantles. It is also found that the H_2O:NH_3 grain mantle ratio prevailing over substantial periods of a cloud lifetime is about 5:1 or higher; e.g. H_2O:NH_3=6:1 for a 2×10^6-year-old cloud of density $n_0=2\times10^4\,cm^{-3}$ and extinction $A_V=4.$ or a 5×10^7-year-old cloud with $n_0=10^5\,cm^{-3}$ and $A_V=8$ (d'Hendecourt, Allamandola & Greenberg 1984).

The 3-μm band of Elias 16 is clearly wider than that of HL Tau and as we have already pointed out can be very well matched by the absorption of an unannealed mixture. Comparing Fig. 9 with Fig. 8 we see that for Elias 16, just as for HL Tau, an appropriate H_2O concentration relative to NH_3 is in the range 5/1 to 6/1. Since Elias 16 is a star which is situated behind the Taurus cloud, the material sampled in the absorption is an average of the cloud dust composition. The high A_V indicates that the average is probably a good one.

The strengths of the various ice bands are a measure not only of the mantle composition but also of its thickness, and are – of course – related to the visual extinction. If we define f as the fraction of H_2O in the molecular mantle mixture and X as the ratio of the ice mantle radius to the compound core radius then we find that the trend of the ratio of the ice absorption to visual extinction τ_3/τ_V is given in Table 2. This table shows the combined trends of variation in mantle composition and grain sizes for unannealed mixtures as well as for annealed mixtures and gives what we consider to be a reasonable representation of what is to be expected under various conditions. The value of τ_3/τ_V is, practically speaking, independent of particle shape.

Although pure ice may occur in very special situations (Hagen, Tielens & Greenberg 1983b) it is highly unlikely in a molecular cloud and therefore the values for $f=1$ are rather severe upper limits.

In Table 3 we have shown the values of τ_{max}, A_V and τ_{max}/τ_V, where $\tau_V=A_V/1.086$. A mean value of this ratio for the cloud is probably best given by Elias 16 and is 0.063. We see in Table 2

Table 2. τ_3/τ_V as function of the ratio A of mantle radius to compound core radius and of the fraction f of H_2O in the mantle mixture.

a. Unannealed ice mixtures:

X\f	0.15	0.20	0.30	0.40	0.50	0.60	0.70	0.80	0.90	1.00
1.1	0.000	0.003	0.009	0.014	0.020	0.026	0.032	0.038	0.043	0.049
1.2	0.000	0.005	0.016	0.027	0.037	0.048	0.059	0.070	0.080	0.091
1.3	0.000	0.007	0.022	0.037	0.052	0.067	0.082	0.097	0.112	0.128
1.4	0.000	0.009	0.028	0.047	0.066	0.085	0.103	0.122	0.141	0.160
1.5	0.000	0.011	0.033	0.056	0.078	0.100	0.123	0.145	0.168	0.190

b. annealed ice mixtures:

X\f	0.15	0.20	0.30	0.40	0.50	0.60	0.70	0.80	0.90	1.00
1.1	0.000	0.004	0.013	0.021	0.030	0.038	0.047	0.055	0.063	0.072
1.2	0.000	0.008	0.023	0.039	0.055	0.071	0.086	0.102	0.117	0.132
1.3	0.000	0.011	0.033	0.055	0.077	0.099	0.121	0.143	0.0164	0.185
1.4	0.000	0.014	0.041	0.069	0.096	0.124	0.152	0.179	0.206	0.233
1.5	0.000	0.016	0.049	0.082	0.114	0.147	0.180	0.213	0.245	0.276

Table 3. Optical depth τ_{max} at the maximum of the absorption band, A_V (from Whittet *et al.* 1983) and the ratio τ_{max}/τ_V for all sources discussed.

Source	τ_{max}	A_V	τ_{max}/τ_V
HL Tau	0.66	6–10	0.072–0.119
XZ Tau	< 0.06	3	< 0.022
Elias 1	0.52	8–10	0.056–0.071
Elias 3	0.41	8.1	0.055
Elias 6	0.41	5.9	0.075
Elias 9	0.14	4.5	0.034
Elias 16	1.19	20.6	0.063

that this corresponds, for example, to a mixture containing 60 per cent H_2O and a mantle approximately 28 per cent larger than the compound core. As has already been shown this size is still well within the range in which the shape of the band is unaffected using our method. We note here that the value of τ_3/τ_V deduced from Fig. 2 in Whittet *et al.* (1983) is about 30 per cent larger, namely 0.084. Using the same mantle–core size ratio of ~1.25, this implies a composition very close to pure H_2O (>80 per cent), which is probably higher than can be expected for any reasonable molecular cloud chemistry (Tielens & Hagen 1982; d'Hendecourt *et al.* 1984). If we use a lower mantle thickness as a mean over the entire cloud, the required composition becomes even more unlikely. It is interesting to observe that a similar calculation for ices in the BN object implies a value of τ_3/τ_V of about 0.05 and an H_2O fraction of about 55 per cent (Greenberg 1982a, b).

8 Conclusion

Our model fitting has shown that comparisons with observations can in a detailed way show evidence for grain and cloud evolutionary properties. We have further shown that by careful analysis we can deduce consistent measures for the absorption strength of such broad features as the 3-μm ice band.

The strengths of the ice bands deduced in this Taurus molecular cloud are quite consistent with strengths deduced from core–mantle grains with expected fractional composition of H_2O.

It is evident that there is a need for more observational data of high quality to determine clear variations in the shape of the ice band features in different environments. These can provide us with deeper insight into the chemical processes in molecular clouds and in the grains themselves.

References

Cohen, M., 1975. *Mon. Not. R. astr. Soc.*, **173,** 279.
Cohen, M., 1983. *Astrophys. J. Lett.*, **270,** L69.
d'Hendecourt, L. B., Allamandola, L. J. & Greenberg, J. M., 1984. *Astr. Astrophys.*, submitted.
Dyke, H. M. & Lonsdale, C. J., 1981. *IAU Symp. No. 96,* p. 223, Reidel, Dordrecht, Holland.
Elias, J. H., 1978. *Astrophys. J.*, **224,** 857.
Greenberg, J. M., 1982a. In: *Comets,* p. 231, ed. Wilkening, L. L., University of Arizona Press.
Greenberg, J. M., 1982b. In: *Submillimetre Wave Astronomy,* p. 261, eds Beckman, J. E. & Phillips, J. P., Cambridge University Press.
Greenberg, J. M., van de Bult, C. E. P. M. & Allamandola, L. J., 1983. *J. Phys. Chem.*, **87,** 4243.
Hagen, W., Tielens, A. G. G. M. & Greenberg, J. M., 1981. *Chem. Phys.*, **56,** 367.
Hagen, W., Tielens, A. G. G. M. & Greenberg, J. M., 1983a. *Astr. Astrophys. Suppl.*, **51,** 389.
Hagen, W., Tielens, A. G. G. M. & Greenberg, J. M., 1983b. *Astr. Astrophys.*, **117,** 132.

Kerker, M., 1969. *The Scattering of Light and Other Electromagnetic Radiation,* Academic Press, New York and London.

Landini, M., Natta, A., Oliva, E., Salinari, P. & Moorwood, A. F. M., 1984. *Astr. Astrophys.,* **134,** 284.

Léger, A., Gauthier, S., Défourneau, D. & Rouan, D., 1983. *Astr. Astrophys.,* **117,** 164.

Merrill, K. M. & Stein, W. A., 1976. *Publs astr. Soc. Pacif.,* **88,** 285.

Shah, G. A., 1970. *Mon. Not. R. astr. Soc.,* **148,** 93.

Tielens, A. G. G. M. & Hagen, W., 1982. *Astr. Astrophys.,* **114,** 245.

van de Bult, C. E. P. M. & Greenberg, J. M., 1984. *Mon. Not. R. astr. Soc.,* **210,** 803.

Whittet, D. C. B., Bode, M. F., Longmore, A. J., Baines, D. W. T. & Evans, A., 1983. *Nature,* **303,** 218.

Willner, S. P., Gillet, F. C., Herter, T. L., Jones, N., Krassner, J., Merrill, K. M., Pipher, J. L., Puetter, R. C., Rudy, R. J., Russell, R. W. & Soifer, B. T., 1982.*Astrophys. J.,* **253.** 174.